1.1 TEM Observation of Dual Ion Beam Irradiated F82H mod.3 and MA957 –T. Yamamoto, Y. Wu, G. R. Odette (University of California Santa Barbara), K. Yabuuchi, A. Kimura (Kyoto University)

OBJECTIVE

The objective of this work is to characterize cavity evolution under Fe^{3+} and He^{+} dual ion beam irradiation in two fusion reactor candidate structural alloys: a normalized and tempered martensitic steel, (TMS) F82H mod.3: and, a nanostructured ferritic alloy (NFA), MA957. The dpa and He/dpa ratio varied with the depth in the sample, but at intermediate locations were ≈ 10 dpa and ≈ 40 appm He/dpa, respectively. The irradiation temperature was 480°C. The dual ion results are compared to in situ He injection experiments in HFIR for similar irradiation conditions, but at a much lower dpa rate.

SUMMARY

TEM microstructures of TMS F82H mod.3 and NFA MA957 have been characterized after dual ion beam (Fe^{3+} and He^{+}) irradiation to a nominal condition of 10 dpa and 400 appm He at ≈ 480°C. The irradiations were performed at dual beam facility, DuET, located at Kyoto University in Japan. Helium bubbles were found at depths greater than 300 nm in F82H mod.3. The average bubble diameter was larger and the number density comparable to or lower than for those observed following in situ He implanter (ISHI) irradiations in the HFIR JP26 experiment at 500°C at similar dpa and He levels (9 dpa and 380 appm He), but at much lower dpa rates. A few larger cavities, that are likely voids, were observed following the DuET irradiation. However, a bimodal bubble and void size distribution was less apparent in the DuET case, compared to the ISHI results. No He bubbles were observed in MA957 following DuET irradiation to a condition similar to that for the JP26 ISHI experiment where bubbles were observed. Bubbles were only visible at DuET conditions of > 15 dpa and He > 550 appm, and they were less numerous than found in the ISHI irradiation at lower damage and He levels.

PROGRESS AND STATUS

Introduction

Predicting and mitigating the effects of a combination of large levels of transmutant He and displacement damage (dpa), produced by high energy neutrons, on the dimensional stability and mechanical properties of structural materials is one of the key challenges in the development of fusion energy [1]. The fundamental overriding questions about He-dpa synergisms include: a) What are the basic interacting mechanisms controlling He and defect transport, fate and consequences, and how are they influenced by the starting microstructure and irradiation variables (dpa rate, He/dpa ratio, temperature and applied stress); and, b) how can the detrimental effects of He-dpa synergisms be mitigated and managed by proper microstructural design?

We have previously demonstrated that in situ He implantation (ISHI) in mixed spectrum fission reactor irradiations provides a very attractive approach to assessing the effects of He-dpa synergisms, while avoiding most of the confounding effects associated with Ni- or B-doping type experiments [1-8]. Another approach to study He-dpa synergism is to use multiple ion beams to simultaneously implant He and create displacement damage with heavy ions [1,9-12]. In spite of an apparent similarity, the two techniques have many differences that include the dpa rate, the spatial distribution of damage and He and the proximity of a free surface. Thus comparing the microstructural evolutions in the same alloys for

the two different irradiation conditions is an important objective and provides a basis to inform, calibrate and validate predictive models.

Experimental Procedure

The alloys studied here are a TMS F82H mod.3 and a NFA MA957. The F82H series is the most widely used TMS alloys for variety of studies including the He effects [1,3,7,11-17]. In the case of F82H mod.3, the base composition of F82H-IEA (nominally, 7.5%Cr 2%W 0.2%V 0.1%C 0.1%Si 0.02%Ta 60ppmN) was modified to reduce N and Ti to 14 ppm and 0.001%, respectively, and to add 0.1% Ta [13]. The steel was austenitized at 1040°C for 30 min, normalized (air-cooled), and tempered at 740°C for 1.5 h. F82H mod.3 has a fine prior-austenite grain size (ASTM 9.5) along with a finer scale lath structure formed in the process of martensitic transformation [13]. MA957 is a representative NFA that is gaining growing interest for the radiation resistance especially with a good He management as well as the good high temperature mechanical properties [1,5,8,18,19]. As-extruded MA957 has a fine scale elongated grain structure with nano-meter scale oxide features (NF) dispersed as strengthening obstacles. The typical grain size is about 1 and 5 μm in the transverse and axial directions, respectively. More details of the materials including the chemical compositions and microstructure are given elsewhere [5,13,18,19].

Two 3 mm diameter disks of the alloys were mechanically ground to a nominal 200 μm thickness were cut into small sections to fit into the ion beam specimen holder. The surface of the section was electro-polished before irradiation. Dual ion beam irradiation was performed in DuET facility in the Institute of Advanced Energy, Kyoto University (Kyoto, Japan), where Fe^{3+} ions accelerated to 6.4MeV by a tandem accelerator and He^{+} ions accelerated to 1MeV by a single end accelerator were simultaneously induced to the specimens held in a temperature control stage [20]. The He+ ion beam was passed through a rotating beam energy degrader that results in He^{+} ions in four energy intervals resulting a broader uniform He deposition profile.

Figure 1 shows depth profile of the displacement damage and He deposition calculated with SRIM 2006 code. The irradiation was performed so that the nominal conditions of 10 dpa and 400 appm He were achieved at the location 600 nm from the specimen surface. The implantation covers a range of He, He/dpa ratios, dpa and dpa rates. The region between ≈ 400 to 1000 nm has an approximately constant 40±5 appm He/dpa ratio, and the region between ≈ 400 and 700 nm accumulated a net dose of ≈ 10±2 dpa. The corresponding dpa rate was ≈ 3 to $6x10^{-4}$ dpa/s. The specimen temperature was controlled at ≈ 480ºC. More generally, the dpa increase to a peak at ≈ 32 dpa at 1600 nm, while the He and He/dpa decrease with increasing depth greater than 1000 nm, approaching 0 at about 1500 nm. Thus, in principle, the DuET irradiation provides a basis to evaluate the effects of a range of irradiation variables, including high dpa with no He as well as undamaged regions.

A FEI HELIOS Focused Ion Beam (FIB) tool was used to micromachine < 100 nm thick electron transparent lift-outs ≈ 5 μm wide and 5 μm deep. Post irradiation TEM was performed on the 200 keV FEI T20 instrument in the UCSB microstructure and microanalysis facility. Through focus bright field imaging used to characterize the cavities. The cavity images were manually marked for location and size and the image analysis software package Image-J was used to determine cavity area number densities and size distributions. The foil thickness, needed to compute volume number densities, was confirmed by convergent beam electron diffraction measurements.

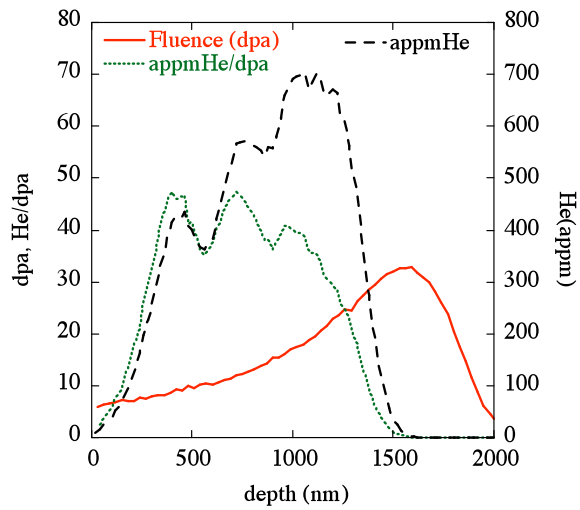

Figure 1. Depth profile of displacement damage and He deposition in the specimens in the DuET dual ion beam irradiation calculated with SRIM 2006 code.

Results and Discussion

Microstructure of dual ion beam irradiated F82H mod.3

Figure 2 shows the low magnification TEM image of the dual ion beam irradiated F82H mod.3 at under-focus condition. Cavities were observed only at the locations between ≈ 300 and 1500 nm from the surface. The 1500 nm corresponds to the He implantation depth. Figure 3 and Figure 4 show high magnification cavity images covering the depths between about 500 to 1000 nm and 1000 to 1500 nm, respectively. The bubbles are strongly associated with dislocations, boundaries and precipitates. The string of pearls arrangements of the bubbles indicate the strong dislocation association. The bubbles on boundaries and precipitates are smaller and more numerous than those formed on dislocations. Significant homogeneous bubble nucleation in the matrix is not observed. The overall bubble sizes are roughly similar in the two regions. A small number of larger faceted cavities with diameters > 7 nm, that are likely voids, are found in the deeper region, corresponding to higher dpa and lower He concentrations and He/dpa ratios.

Figure 5 shows the average diameter and number density as a function of depth. These analyses were performed for the areas sectioned in 100 nm steps so that, for example, the data for 400 nm represents the area at a depth from 400 to 500 nm. The significant "scatter" is largely due to variations in the local microstructure. There is a slight general trend to a decrease in the average diameter of the bubbles with depth that may be due to the irradiation conditions. The average diameter of the bubble at a depth of 600 nm is ≈ 4 nm. The corresponding number densities are lower up to about 700 nm with values of ≈ $4.5\pm1\times10^{22}/m^3$, followed by a peak density of ≈ $1.2\times10^{23}/m^3$ at 800 nm that is then followed by a decrease at greater depths up to the end of the He deposition range.

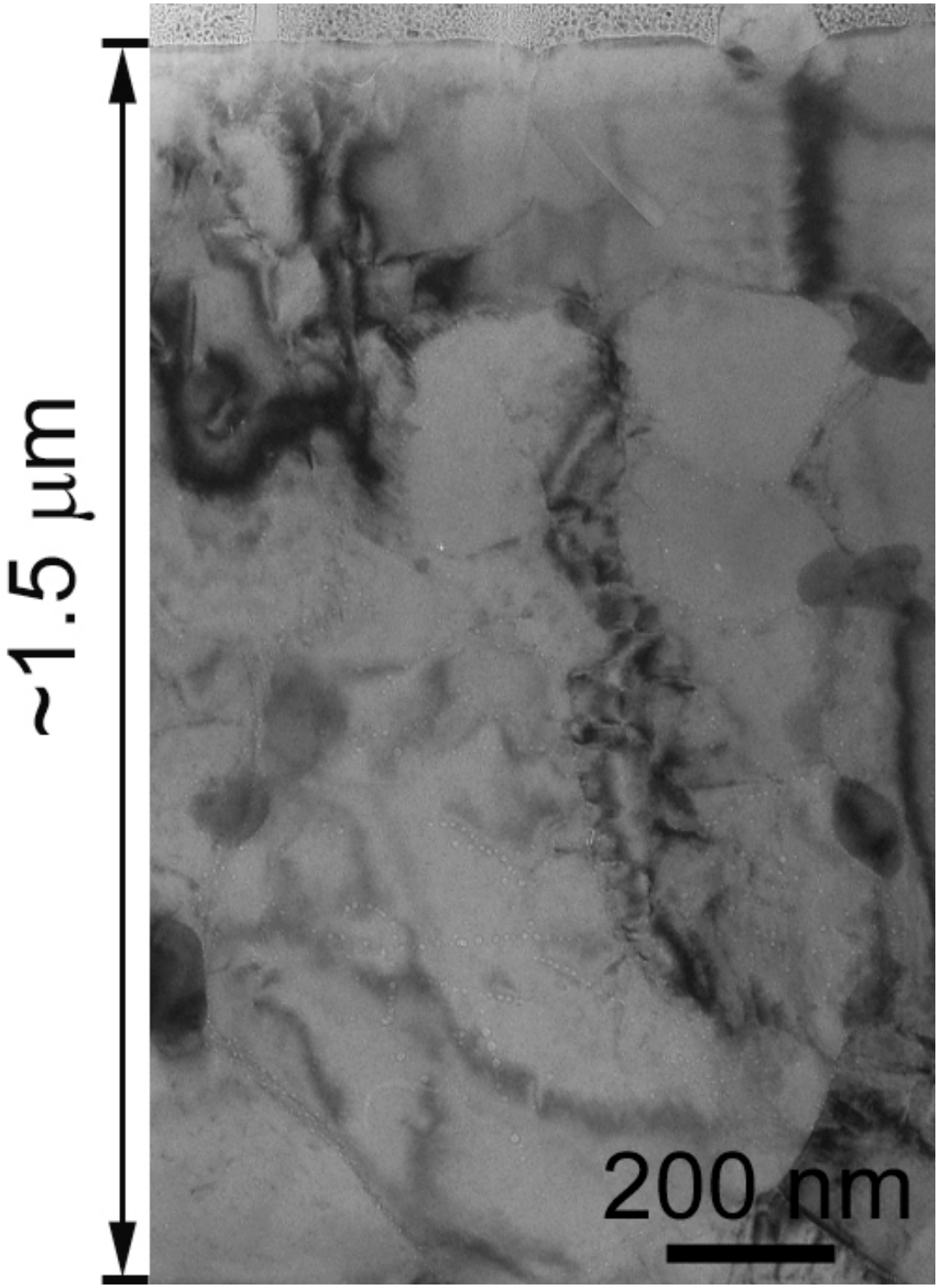

Figure 2. Low magnification under-focused TEM image showing He bubbles in F82H mod.3 after dual beam irradiation over the He deposition zone.

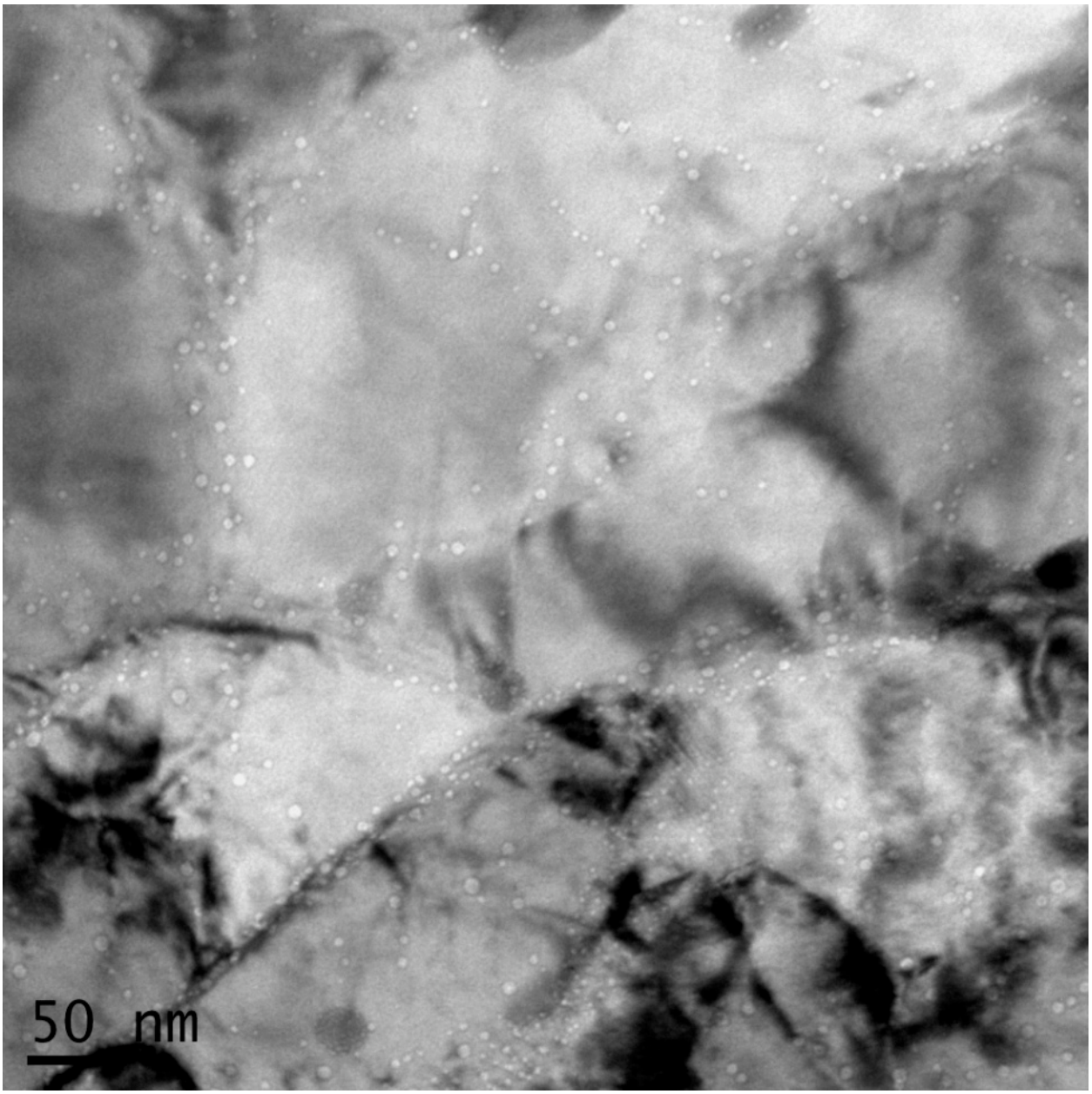

Figure 3. High magnification under-focused cavity image showing He bubbles in F82H mod.3 after dual ion beam irradiation in the area located from ≈ 0.5 to ≈ 1.0 μm deep from the surface.

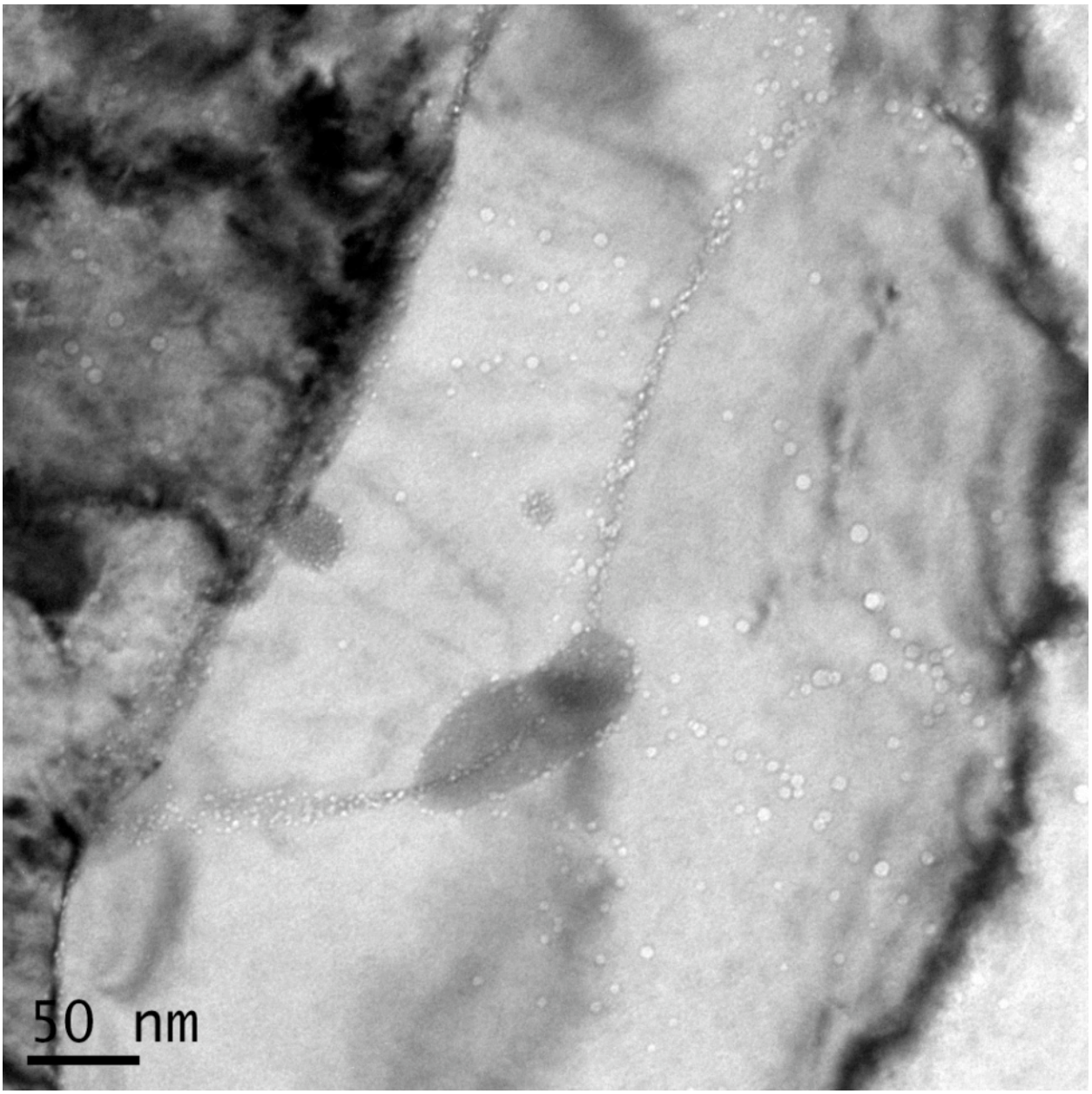

Figure 4. High magnification under-focused cavity image showing He bubbles in F82H mod.3 after dual ion beam irradiation in the area located from ≈ 1.0 to ≈ 1.5 μm deep from the surface.

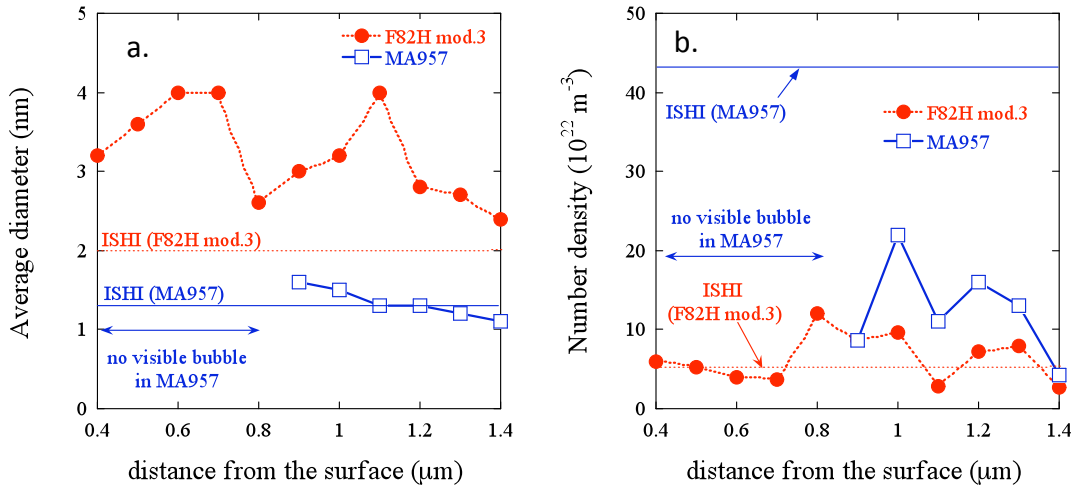

Figure 5 (a) Average diameter and (b) number density of He bubbles as a function of the distance from the surface for F82H mod.3 and MA957 after DuET irradiation. Analyses were conducted for the areas sectioned by 0.1 μm step so that, for example, 0.4 μm distance analysis covers the area from 0.4 to 0.5 μm in the distance. Thin horizontal lines show the results from ISHI experiments for the alloys.

TEM observation of the same alloy irradiated in the ISHI HFIR irradiation to approximately same dpa and He condition (9 dpa, 380 appm He) nominally at 500°C, showed a somewhat smaller average cavity size that has been reported to range from ≈ 2 to 3.4 nm [6,7,THIS STUDY], compared to that observed at 400-600 nm in the DuET irradiation condition of ≈ 3.7±0.3 nm. The corresponding nominal ISHI number densities of 5.3×10^{22} m^{-3}, are similar to that for the DuET irradiation at 600 nm ≈ $4.5\pm0.5\times10^{22}$ [5]. However, these comparisons require a caveat. The ISHI and DuET studies were carried out at different times and by different researchers, using somewhat different techniques. Thus it will be important to repeat the characterization of the cavity structures for the ISHI conditions using methods that are identical to those used for the DuET irradiations. Further, the characterization must develop metrics that account for the local microstructural-bubble associations and the corresponding variations noted above.

Indeed the comparison of ISHI and DuET cavity structures shown in Figure 6 suggest more significant differences that described above. In both cases, the regions examined are dominated by dislocation-associated bubbles. The ISHI irradiation clearly has a higher density of smaller (see Figure 6a) bubbles compared to the DuET irradiation condition. Further, a bimodal cavity distribution composed of small bubbles and large voids is observed in the ISHI condition, while the distribution is more unimodal for the DuET irradiation.

Microstructure of the DuET irradiated NFA MA957

As shown in Figure 5, bubbles are not observed in the DuET irradiation condition of MA957 at a depth of less than 800 nm. Figure 7a and b show under-over focus TEM images of the DuET irradiated MA957 from ≈ 900 to ≈ 1100 nm. A high density (≈ 1.5×10^{23}/m^3) of small bubbles with average diameter of ≈ 1.4 nm were observed; and larger faceted voids were entirely absent in this case. As shown in Figure 7c the bubbles in MA957 are much smaller than in F82H mod.3. The dpa at this depth is ≈ 15 to 20 dpa. While

the sizes are similar, the bubble number density in the DuET irradiation (≈ $1.5 \times 10^{23}/m^3$) is about a factor of 3 lower than for the ISHI condition ($4.3 \times 10^{23}/m^3$).

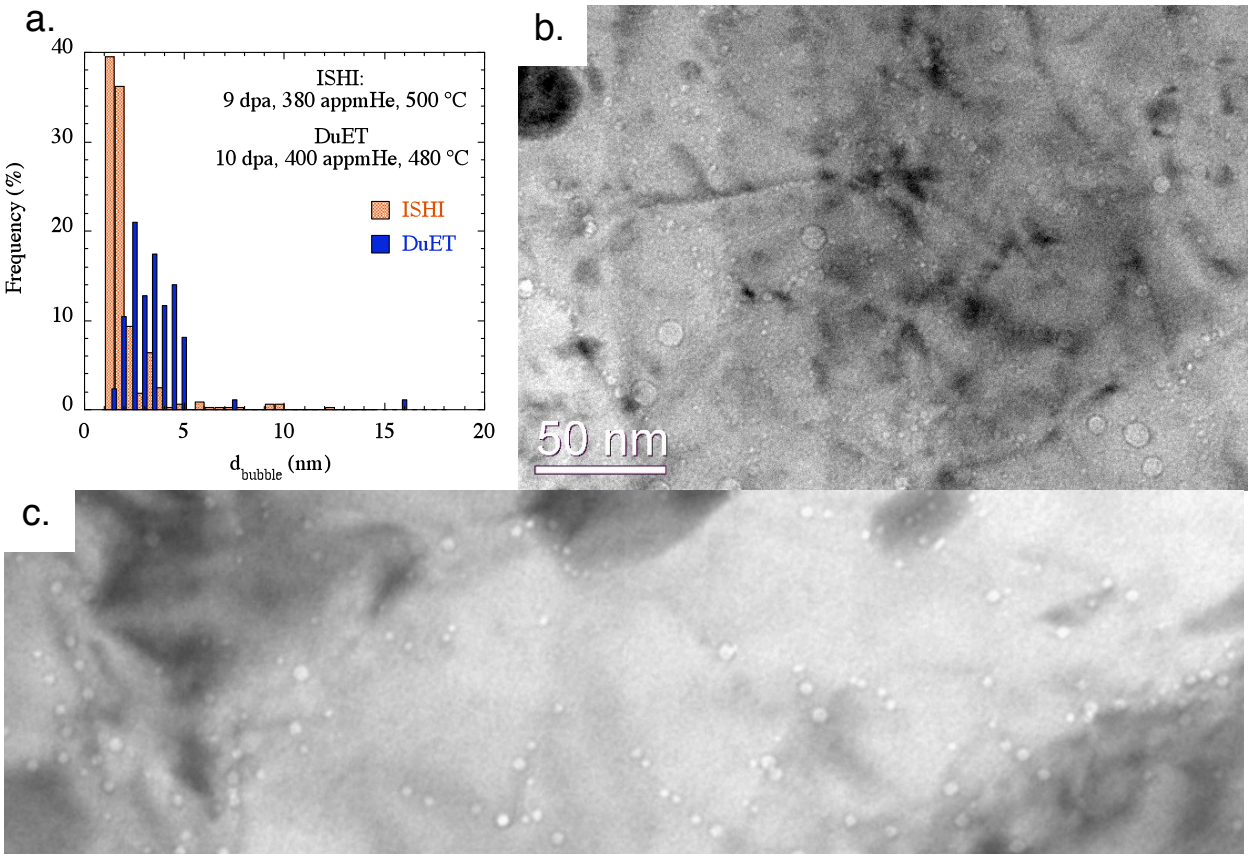

Figure 6. (a) Comparison of the He bubble size distributions in F82H mod. 3 specimens irradiated and He implanted in ISHI experiment vs. DuET facility; and corresponding bubble microstructure images in (b) ISHI and (c) DuET irradiation. Two TEM images are at the same magnification.

Future Research

Work during the current reporting period will include continued evaluation of the cavity and other microstructures in both the DuET and ISHI irradiation conditions. Further, the nominal comparative dpa in the DuET irradiations will be extended to ≈ 25 dpa and 1000 app He. ISHI specimens irradiated to a similar peak dpa and He content from the HFIR JP27 experiment will also be examined.

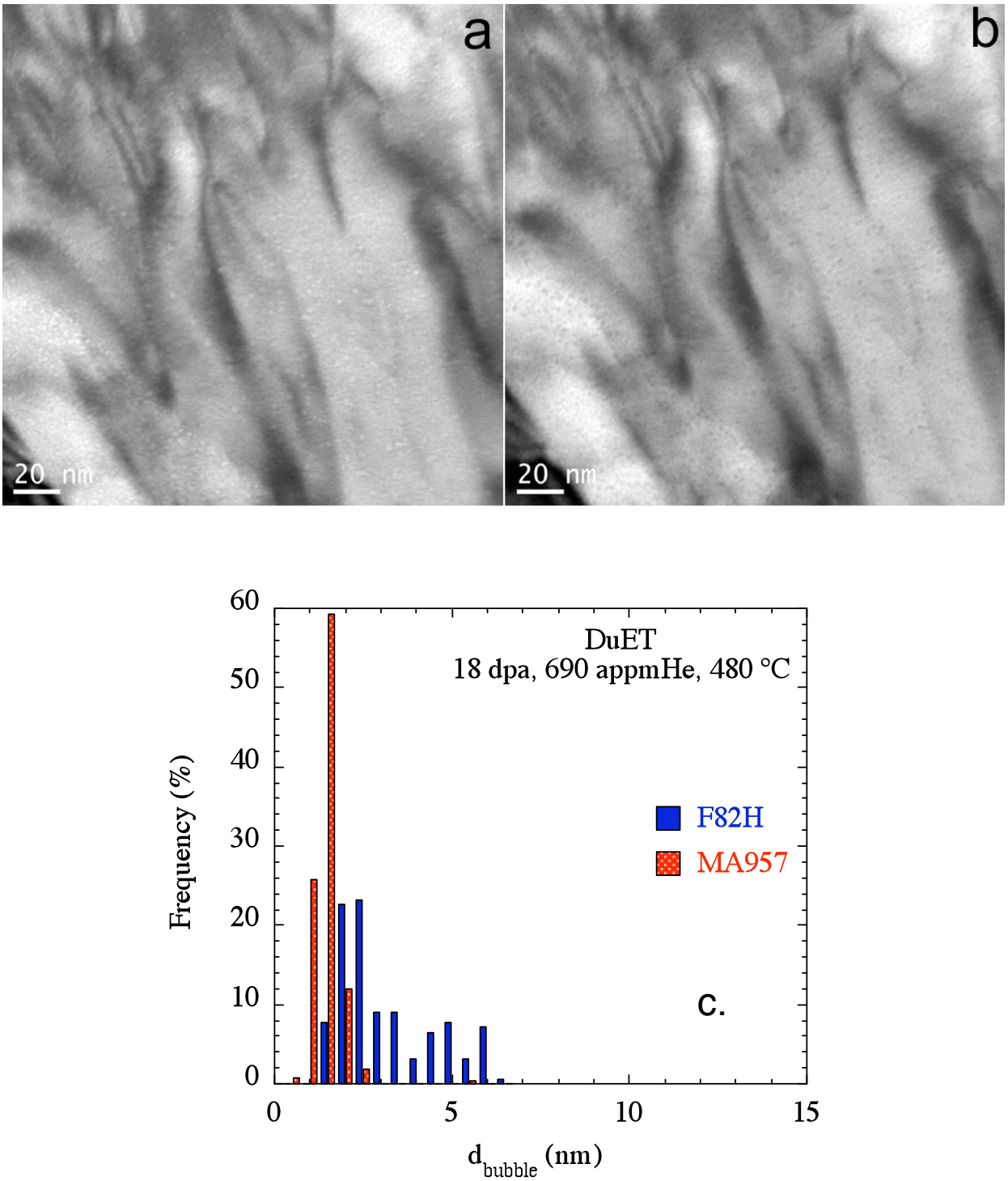

Figure 7. (a) an under focus and (b) an over focus TEM images of MA957 irradiated and He implanted in DuET irradiation over the depth range about 0.9-1.1 μm. (c) bubble size distributions over the depth range 1.0 - 1.1 μm in MA957 and F82H mod.3.

Acknowledgements

This work has been conducted as a part of the TITAN program for US DOE- Japan MEXT collaboration for fusion energy research. The work performed at UCSB was supported by the U. S. Department of Energy, Office of Fusion Energy Sciences, under contract DE-FG03-94ER54275.

References

[1] Y. Dai, G.R. Odette, T. Yamamoto, *The Effects of helium on irradiated structural alloys (2011) in press.*
[2] T. Yamamoto, G. R. Odette, L. R. Greenwood, *Fusion Materials Semiannual Report 1/1 to 6/30/2005* DOE/ER-313/38 (2005) 95.
[3] T. Yamamoto, G. R. Odette, P. Miao, D. T. Hoelzer, J. Bentley, N. Hashimoto, H. Tanigawa, R. J. Kurtz, J. Nucl. Mater. 367 (2007) 399.
[4] R. J. Kurtz, G. R. Odette, T. Yamamoto, D. S. Gelles, P. Miao, B. M. Oliver, *J. Nucl. Mater.* 367-370, 417 (2007).
[5] G. R. Odette, M. J. Alinger, B. D. Wirth, Annu. Rev. Mater. Res. 38 (2008)471.
[6] T. Yamamoto, G. R. Odette, P. Miao, D. J. Edwards, R. J. Kurtz., J. Nucl. Mater. 386-388 (2009) 338.
[7] D. J. Edwards, R. J. Kurtz, G. R. Odette, T. Yamamoto, *Fusion Materials Semiannual Report 12/31/2009* DOE/ER-313/47 (2010) 59.
[8] G. R. Odette, P. Miao, D. J. Edwards, T. Yamamoto, R. J. Kurtz, Y. Tanigawa, J. Nucl. Mat. (2011) in press.
[9] E. H. Lee, J. D. Hunn, T. S. Byun, L. K. Mansur, J. Nucl. Mater. 280 (2000) 18.
[10] H. Kishimoto, K. Yutani, R. Kasada, A. Kimura, Fusion Eng. Des. 81 (2006) 1045.
[11] R. Kasada, H. Takahashi, H. Kishimoto, K. Yutani, A. Kimura, *Materials Science Forum 654-656* (2010) 2791 (*doi:10.4028/www.scientific.net/MSF.654-656.2791).*
[12] A. Kimura, R. Kasada, A. Kohyama, H. Tanigawa, T. Hirose, K. Shiba, S. Jitsukawa, S. Ohtsuka, S. Ukai, M. A. Sokolov, R. L. Klueh T. Yamamoto, G. R. Odette, J. Nucl. Mater. 367-370 (9007) 60.
[13] K. Shiba, M. Enoeda, S. Jitsukawa, J. Nucl. Mater. 329-333 (2004) 243.
[14] A. Kimura, R. Kasada, K. Morishita, R. Sugano, A. Hasegawa, K. Abe, T. Yamamoto, H. Matsui, N. Yoshida, B. D. Wirth, T. D. de la Rubia, J. Nucl. Mater. 307-311 (2002) 521-526.
[15] G. R. Odette, T. Yamamoto, H. J. Rathbun, M. Y. He, M. L. Hribernik, J. W. Rensman*, J. Nucl. Mater.* **323** (2003) 313.
[16] T. Yamamoto, G. R. Odette, H. Kishimoto, J-W. Rensman, P. Miao, *J. Nucl. Mater.* **356** (2006) 27.
[17] Z. Tong, Y. Dai, J. Nucl. Mater. 385 (2009) 258.
[18] M. L. Hamillton, D. S. Gelles, R. J. Lobsinger, M. M. Paxton, W. F. Brown, "Fabrication Technology for ODS Alloy MA957," PNL-13165, Pacific Northwest Laboratory (2000).
[19] Y. Wu et al. to be published.
[20] A. Kohyama, Y. Katoh, M. Ando, K. Jimbo, Fusion Eng. Des. 51-52 (2000) 789.